



Coking and decoking chemistry for resource utilization of polycyclic aromatic hydrocarbons (PAHs) and low-carbon process

Nan Wang^{a,d}, Li Wang^c, Yuchun Zhi^a, Jingfeng Han^a, Chengwei Zhang^{a,d}, Xinqiang Wu^a, Jinling Zhang^a, Linying Wang^a, Benhan Fan^{a,d}, Shutao Xu^a, Yijun Zheng^a, Shanfan Lin^{a,d}, Renan Wu^c, Yingxu Wei^{a,*}, Zhongmin Liu^{a,b,d,*}

^a National Engineering Research Center of Lower-Carbon Catalysis Technology, Dalian National Laboratory for Clean Energy, iChEM (Collaborative Innovation Center of Chemistry for Energy Materials), Dalian Institute of Chemical Physics, Chinese Academy of Sciences, Dalian 116023, Liaoning, China

^b State Key Laboratory of Catalysis, Dalian Institute of Chemical Physics, Chinese Academy of Sciences, Dalian 116023, Liaoning, China

^c Laboratory of High-Resolution Mass Spectrometry Technologies, CAS Key Laboratory of Separation Science for Analytical Chemistry, Dalian Institute of Chemical Physics, Chinese Academy of Sciences, Dalian 116023, Liaoning, China

^d University of Chinese Academy of Sciences, Beijing 100049, China

ARTICLE INFO

Article history:

Received 8 July 2022

Revised 25 August 2022

Accepted 7 September 2022

Available online 13 September 2022

Keywords:

Methanol-to-olefins

SAPO-34

Polycyclic aromatic hydrocarbons (PAHs)

Catalyst deactivation

Catalyst regeneration

Low CO₂ emission

ABSTRACT

Low-carbon process for resource utilization of polycyclic aromatic hydrocarbons (PAHs) in zeolite-catalyzed processes, geared to carbon neutrality—a prominent trend throughout human activities, has been bottlenecked by the lack of a complete mechanistic understanding of coking and decoking chemistry, involving the speciation and molecular evolution of PAHs, the plethora of which causes catalyst deactivation and forces regeneration, rendering significant CO₂ emission. Herein, by exploiting the high-resolution matrix-assisted laser desorption/ionization Fourier-transform ion cyclotron resonance mass spectrometry (MALDI FT-ICR MS), we unveil the missing fingerprints of the mechanistic pathways for both formation and decomposition of cross-linked cage-passing PAHs for SAPO-34-catalyzed, industrially relevant methanol-to-olefins (MTO) as a model reaction. Notable is the molecule-resolved symmetrical signature: their speciation originates exclusively from the direct coupling of in-cage hydrocarbon pool (HCP) species, whereas water-promoted decomposition of cage-passing PAHs initiates with selective cracking of inter-cage local structures at 8-rings followed by deep aromatic steam reforming. Molecular deciphering the reversibly dynamic evolution trajectory (fate) of full-spectrum aromatic hydrocarbons and fulfilling the real-time quantitative carbon resource footprints advance the fundamental knowledge of deactivation and regeneration phenomena (decay and recovery motifs of autocatalysis) and disclose the underlying mechanisms of especially the chemistry of coking and decoking in zeolite catalysis. The positive yet divergent roles of water in these two processes are disentangled. These unprecedented insights ultimately lead us to a steam regeneration strategy with valuable CO and H₂ as main products, negligible CO₂ emission in steam reforming and full catalyst activity recovery, which further proves feasible in other important chemical processes, promising to be a sustainable and potent approach that contributes to carbon-neutral chemical industry.

© 2022 Science Press and Dalian Institute of Chemical Physics, Chinese Academy of Sciences. Published by ELSEVIER B.V. and Science Press. All rights reserved.

1. Introduction

Catalyst deactivation, caused by carbonaceous deposits or “coke”, is ubiquitous in the field of heterogenous catalysis utilizing zeolites and/or metal oxides, which forces regeneration or, in the worst-scenario, replacement of coked catalysts, resulting in significant economic and resource losses in the chemical sector world-

wide [1]. Coke has commonly been removed by combustion in air [2]. However, this leads to an increased consumption of fossil resources and, in particular, massive carbon dioxide (CO₂) emission into the atmosphere, inducing the serious greenhouse effect and climate issues that require addressing globally. Thus, the pursuit of ecofriendly regeneration strategies in catalytic industry is appealing and significant for sustainable chemistry and carbon neutrality. On the other hand, coke containing significant energy in the form of mixture of aromatics and polycyclic aromatic hydrocarbons (PAHs), if utilized, would become potential carbon

* Corresponding authors.

E-mail addresses: weiyx@dicp.ac.cn (Y. Wei), liuzm@dicp.ac.cn (Z. Liu).

resources for the production of platform compounds and fine chemicals. Accordingly, to deploy rational design of the future-generation industrial catalyst regeneration strategy mingling zero CO₂ emission with resource utilization of PAHs has currently become a pressing concern for both academia and industry; systematic and complete mechanistic understanding of coking and decoking chemistry is the prerequisite for alleviating coke formation and reducing CO₂ emission.

In zeolite catalysis chemistry, though dwelling in a confined space is a restricted privilege that nanoconfinement synergizing with the shape-selective effect appreciably improves the selective production of targeted products, it *per se* imprisons more massive PAHs [3]. Such interaction leads to the molecular evolution of confined PAHs and the formation of complex network of coke species, complicating the chemistry of coking. One exemplar is the SAPO-34 catalyzed methanol-to-olefins (MTO) reaction, which since the first commercialization in 2010, has become a vital non-petroleum route for light olefins production from alternative resources including coal, natural gas, and also biomass and CO₂ as starting feedstock [4,5]. One hallmark is that this heterogeneous catalytic process proceeds through the sophisticated hydrocarbon pool (HCP) concept based on a distinctive shape selectivity principle with the selective production of gas-phase light olefins and the formation of carbonaceous species confined inside the zeolite nanospace in a cavity-controlled manner [3,6–8]. Despite not as the main products, it is the mysterious carbonaceous species and their ever-evolving dynamic inherency under the confinement that endow the consequent organic–inorganic supramolecular cocatalytic center-composed of themselves and the surrounding zeolite microenvironments-with unique autocatalytic properties, working as the real catalyst, accelerating methanol conversion [7,9,10]. Concurrently, their continuous formation and evolution are exacerbated, and eventually they terminate as inactive PAHs [11,12], the plethora or excessive condensation of which would hinder mass transfer [13], thereby causing SAPO-34 catalyst deactivation (decay of autocatalysis) within hours. In this regard, the dynamic evolution of confined hydrocarbons makes coking chemistry in zeolites more complicated. Therefore, to alleviate coking and to regenerate deactivated catalysts through decoking, unambiguously fingerprinting the mechanistic pathways of evolution from active HCP species (e.g., polymethylbenzene) to inactive PAHs (e.g., pyrene and more condensed PAHs), disentangling the complex evolution network composed of intertwined conversion routes of the confined hydrocarbons (especially PAHs), thereof establishing a comprehensive molecule-resolved interpretation of the coking and decoking chemistry, and further achieving a holistic understanding of the decay and recovery mechanisms of dynamic autocatalytic behaviors under the zeolite confinement are necessitated. Furthermore, the stories about the interplay of the zeolite confined space, zeolite catalysis and C1 chemistry would bridge the catalyst materials design and industrial process development.

Most insights have been yielded from the previously established method [14] and spectroscopic studies, including infrared [15,16], UV-Raman [17–20], ultraviolet-visible [11], and NMR spectroscopy [21,22], some of which were operated under *in situ* or operando modes, as well as from theoretical simulations [23,24]. Although these studies have explored the mechanism of the formation of initial C–C bond containing species [25–32], build-up of HCP species and the evolution of HCP species towards coke [33–35], studies that can truly discriminate between active HCP species and deactivating PAHs and the focus on insoluble fraction of coke, especially on their molecular evolution, are rather limited. Yet, these highly condensed PAHs, as the crucial end-product of carbon resources, are the most critical issue of coking chemistry. Molecular deciphering of their speciation and dynamic evolution are the criteria for deactivation and prerequisites for new regener-

ation strategy development. It is therefore vital to bridge the knowledge gap regarding the formation of insoluble coke and molecular routes of PAHs in zeolite confined space, so as to establish a complete framework for coking chemistry, especially in industrial-relevant catalytic systems, involving industrial catalysts and fluidized bed reactors [4].

Cofed water or steam-involved applications are prevalent in chemical industry, yet in-depth studies investigating the mechanistic roles of cofed water in mitigating coking and prolonging catalyst lifetime so far remain elusive. Ruiz-Martínez et al, by combining advanced molecular dynamics simulations with *in situ* microspectroscopy, revealed that the proton mobility largely influenced by water competitive adsorption at acid sites at 330 °C moderates the formation of HCP species, inducing a more homogenous coke distribution and a more efficient use of the SAPO-34 catalyst crystallite [36]. Even the long-term concern from industry and academy, mechanistic fingerprints are still lacking on how water retards aromatic extension and hinders the PAHs clustering (insoluble coke formation) in industrial catalytic processes. On the other hand, PAHs steam reforming over metal-supported catalysts at high temperatures (over 700 °C) has received substantial attention and is considered an efficient approach to removing tar in biomass conversion [37], whereas research on steam reforming of PAHs over zeolite materials is scant. A very recent study reported the direct transformation of coke into naphthalene by steam over SAPO-34 [38]. However, the underlying mechanism and molecular evolution routes of water-induced PAHs decomposition remain unrevealed, and a complete interpretation of decoking chemistry is far from being achieved.

Herein, we take the SAPO-34-catalyzed MTO reaction under industrial-relevant condition as a model reaction. By exploiting the state-of-the-art high-resolution MALDI FT-ICR mass spectroscopy, we unveil the missing fingerprints of the mechanistic pathways for both formation and decomposition of the cross-linked cage-passing PAH clusters in SAPO-34 confined space. Molecular deciphering and fulfilling the full-spectrum MTO products molecular evolution trajectory leads us to a complete molecular understanding of the chemistry of coking and decoking in zeolite catalysis. By elucidating and leveraging the positive yet divergent roles of water in alleviating coking and promoting coke decomposition, we propose a steam regeneration strategy with H₂ and CO as main products and full recovery of catalyst reactivity, enabling resource utilization of PAHs and zero CO₂ emission in coke steam reforming (Fig. 1), which is later proved feasible in the important FCC process. This ecofriendly approach for industrial catalyst regeneration would potentially contribute to carbon neutrality in the chemical sector globally.

2. Results and discussion

2.1. Full-spectrum evolution of MTO reaction products

Starting from methanol, MTO reaction produces gas-phase hydrocarbons dominated by light olefins, and at the same time carbonaceous species deposited in zeolite confined space, together constituting a full spectrum of MTO conversion. Macroscopically, the formation of light olefins is regarded as the primary reaction and other as side reactions. To fulfill the full-picture evolution decoding, unequivocal molecular deciphering of “coke” is the essential prerequisite. However, spatiotemporal inhomogeneity of MTO reaction and coking along the catalyst bed caused by axial and radial methanol concentration gradients and local overheating [39,40] would significantly erode the accuracy of coke structure identification and quantitative analysis. To bypass such inhomogeneous deactivation, when performing MTO reactions in this work

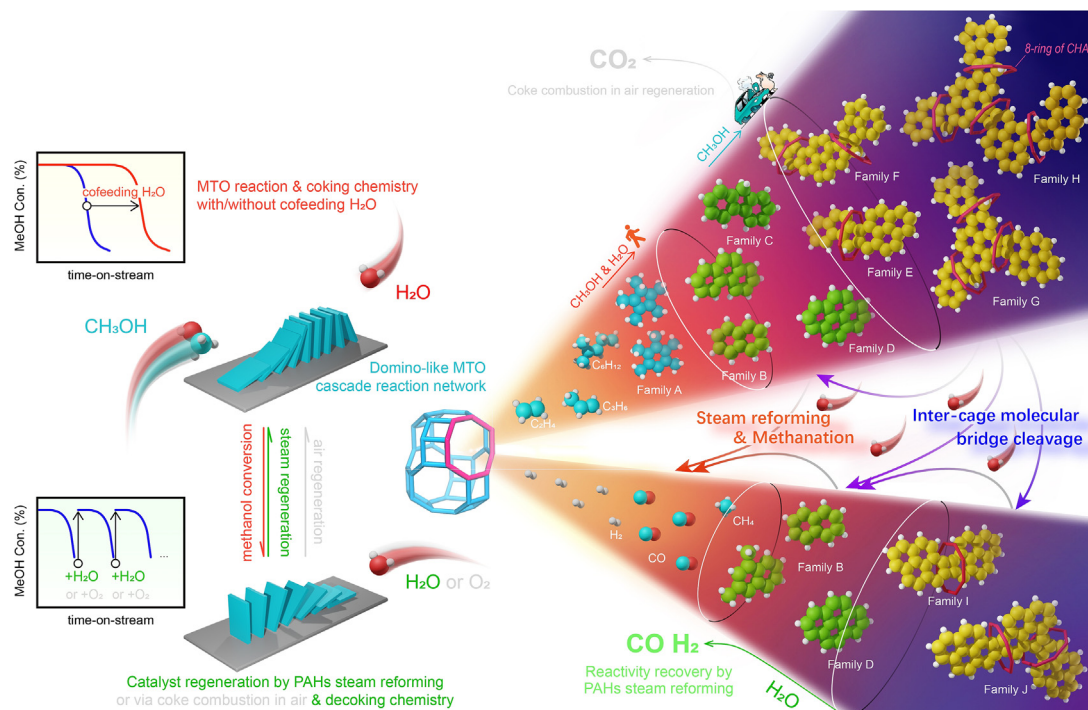


Fig. 1. A schematic compiling the molecule-resolved interpretation of full-spectrum MTO products evolution trajectory as well as the coking chemistry for MTO reaction over SAPO-34 and decoking chemistry for steam regeneration. Cofed water mitigates domino-like MTO cascade reaction network and prolongs catalyst lifetime by retarding PAHs extension and clustering while coked catalyst is regenerated by water under hydrothermal conditions via the steam-promoted PAHs decomposition into H_2 and CO , instead of CO_2 . The steam regeneration strategy proposed herein mingles resource utilization of PAHs and avoiding CO_2 emission from combustion, contributing to a circular carbon atom economy as well as carbon neutrality in the chemical sector.

we employed the fluidized-bed reactor featuring superior mass transfer and heat transfer efficiency. In addition, homogeneous coke distribution at the particle scale is equally crucial. To this end, we employed the shaped fluidized-bed MTO catalyst, in the particle of which HSAPO-34 are dispersed in inert porous binders (see physicochemical properties in Fig. S1).

As shown in Fig. S2, uniform MTO reaction and coking phenomena appeared for water cofeeding MTO reaction over the MTO catalysts at 475°C and methanol weight hourly space velocity (WHSV) of 1.5 h^{-1} . The catalytic performance evaluated by effluent products is presented in Fig. 2(a). A slight induction period—unusual at such high reaction temperature—occurred in the initial 24.5 min of the reaction, implying that the incipient HCP species build-up was suppressed by cofed water, insufficient to trigger methanol fully converted. This is confirmed by the rather less “coke” signals detected after 3 min (Fig. 2b and c). Ethene and propene continued to grow as major effluent products with their selectivity reaching the maximum at 153.5 min, and thereafter, methane gradually dominated the effluents. Methanol started to appear in the effluents after 153.5 min, followed by a rapid catalyst deactivation, signifying the accessibility of acid sites at SAPO-34 micropore to methanol was severely hampered by “coke” deposition, unable to sustain full methanol conversion [41]. This was well-supported by the specific micropore surface area and micropore volume significantly dwindling by ca. 85% (Table S1) correlated with an almost linear increase of coke content before 153.5 min (Fig. 2e).

Prior to the identification of chemical nature of “coke” molecules, we first clarify where coke accommodates. As shown in Fig. S3, without dissolving the framework by hydrofluoric acid, no remarkable coke MS peak signals were detected in the direct test of spent catalysts using the state-of-the-art MALDI FT-ICR MS. In stark contrast to the massive external surface coke signals

identified by applying similar method on coked HZSM-5 [42] and HBEA [43], this absence of coke signals precludes the possibility of appreciable catalytically consequential extents of coking occurrence on the external surface of HSAPO-34 crystals or “coke” migration from the micropore voids to crystal external surface or porous binder. Of further note, the surprisingly high mesopore volume of catalyst (accounting for ca. 20% of the total pore volume, mainly contributed by porous binder) remains virtually identical with the proceeding of the reaction, further negating mesopore formation under the impact of cofed water [44]. Besides, the negative correlation between the micropore volume and the “coke” content before 196.5 min (Fig. S4) also implies the selective filling of “coke” inside the micropore voids.

Next, we commence our experiments with the precise full-picture “coke” molecular structure deciphering. As illustrated in Fig. S6 and Table S2, speciation of coke deposits in SAPO-34 confined space from methanol conversion is extremely complicated compared to largely and highly-selectively produced ethene and propene as the main among the effluents. The CCl_4 soluble fractions (termed as soluble “coke”, ranging from polymethylbenzenes to pyrene) characterized by gas chromatograph-mass spectrometry (GC-MS) are denoted in order as Families A to D according to the growing number of benzene ring structures in the polyaromatics; whereas the residual heavier counterparts (insoluble coke) are definitely identified as cross-linked cage-passing multicore PAHs and are denoted in order as Families E to H according to the increasing number of the proximal cages occupied, by using MALDI FT-ICR MS coupled with isotope labeling technique (see Fig. S7 and Table S3 for detailed identification procedure). This integrated strategy was originally proposed in our previous study [12], and these cage-passing PAHs were found with identical structural identities as the coke in the fixed-bed reaction (Fig. S6). As reaction proceeded, the proportion of soluble “coke” declined monotonously

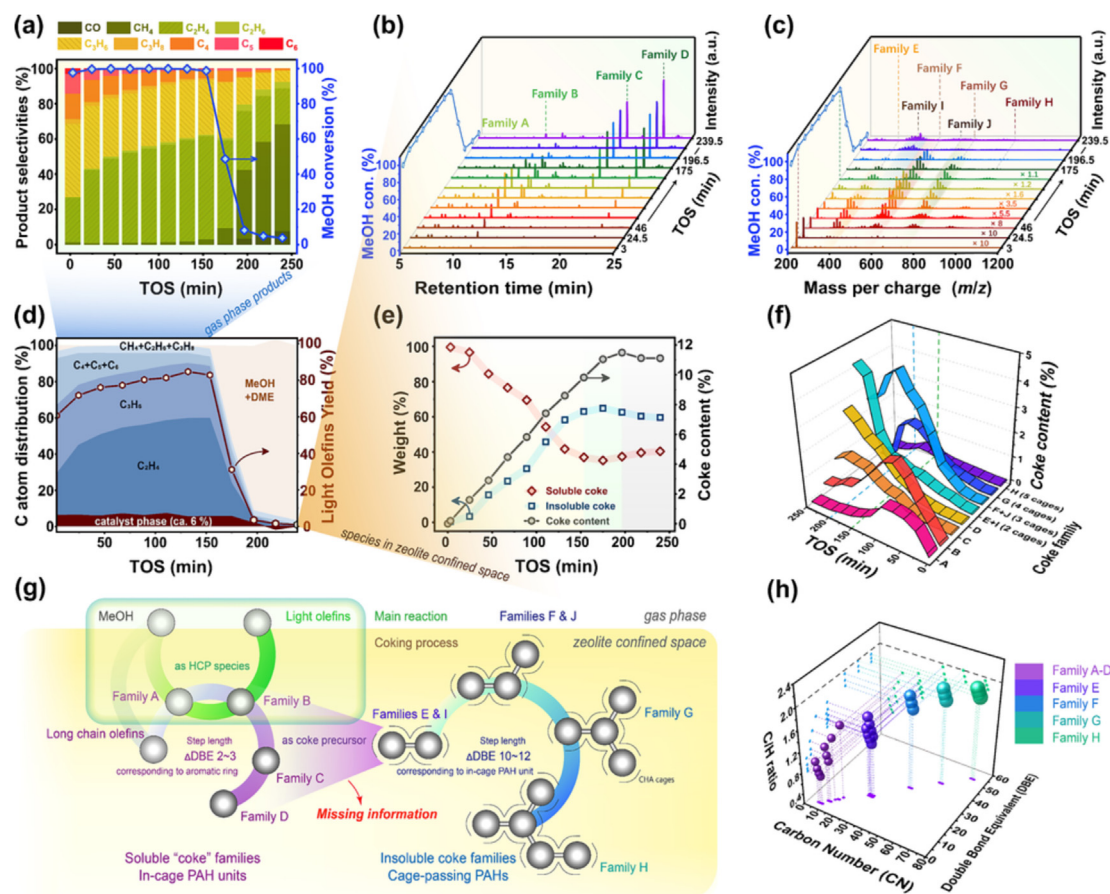


Fig. 2. Catalytic performance of methanol conversion and full-spectrum products analyses. (a) Cofeeding water MTO performance elevated by gas-phase products over MTO catalyst at 475 °C and WHSV of 1.5 $\text{g}_{\text{MeOH}} \text{g}_{\text{cat}}^{-1} \text{h}^{-1}$. Time-evolving gas chromatograms of the CCl_4 soluble fractions of the retained organics (soluble “coke”, b) and MALDI FT-ICR mass spectra of the liberated carbonaceous deposits (insoluble coke, c) from the catalysts after MTO reaction for different durations. (d) Full-spectrum MTO products with real-time carbon atom footprints distribution (CAFD) taking both gas-phase hydrocarbons and “coke” species confined in SAPO-34 nanospace into account simultaneously. (e) Total coke content with time-on-stream (TOS) and weight percentage of soluble “coke” and insoluble coke. (f) Accumulative content of overall “coke families” with TOS. (g) A schematic overview of the full-spectrum molecular evolution routes, featuring an increasing iterative DBE step length, spanning from gas-phase olefins to flowing HCP species (long chain olefins occluded) to soluble “coke” confined in individual cavities (ranging from Families A to D) and eventually to the more condensed insoluble cage-passing PAHs (ranging from Families E to J). (h) The 3D plot of double bond equivalent (DBE) and C/H ratio of each “coke” family against carbon number (CN) increment.

from 100% while the insoluble coke moieties continued to increase and accounted for over 60% before complete deactivation (Fig. 2e). These observations reveal that the extension and cross-linked clustering of occluded HCP species are spontaneous and persistent. To attain thorough insights of coking in zeolite confined space and its chemistry, special attention must be paid to the missing fingerprints of the critical mechanistic pathways for PAHs formation, not merely qualitatively, but specially quantitatively.

Herein, a quantitative methodology was upgraded based on the results from control experiments using model compounds as reference (Fig. S8). The valuable quantitative deconvolution of each insoluble PAH species is hence acquired for the first time, whereby more crucially, the complex full-spectrum “coke” family evolution routes can be quantitatively tracked in real time. As plotted in Fig. 2(f), after a rapid accumulation of phenyl- and naphthyl-species (Families A and B) as HCP species in the initial 89 min of the reaction, the formation of phenanthryl- and pyrenyl-species (Families C and D) occurred at the expense of the decrease in HCP species. These quantitative observations signify that the propensity of organic intermediates towards coke precursors via aromatic extension gradually trumped that to act as HCP species. Concurrently, the transition of catalyst from the high-efficient stage to a less active stage initiated. Thereafter, the rapid accumulation of the more condensed cage-passing PAHs (Families E to H)

occurred in accompany with a sharp decrease in methanol conversion at 175 min (Fig. 2a), revealing a direct correlation between their speciation and the intensification of catalyst deactivation. According to DFT-based configurational optimization, as shown in Fig. S6, the archipelago-structured cage-passing multicore PAHs present single-layer graphene-like architecture, mostly oriented parallel to the 6-rings and traverse (occupy) the 8-ring windows, the latter of which are the main location for Brønsted acid sites and diffusion admittance for methanol [13]. We propose, therefore, that deactivation of CHA zeolite materials occurs through local cage blocking, not solely by extended polyenes [45], adamantane [46,47] and pyrene [34] occluded in individual cages, but more significantly, with their cross-linked coupling, being accelerated by the cage-passing PAH clusters. This dynamic coke motif may account for the steep inverse S-shaped conversion profile in CHA materials at higher temperatures, in contrast to the relatively gentle deactivation curves obtained at lower temperatures [12] or in zeolite ZSM-5 [42,48–50], where PAHs cross-linking behaviors are less pronounced.

In light that the complex “coke” families confined in the zeolite nano-environment are generated from the transformation of the light hydrocarbon products [6,7,10,51], further, based on the above quantitative measurement of insoluble coke, we proposed a carbon atom footprints distribution (CAFD) model, by tracing the carbon

atom footprints from C1 methanol into each converted hydrocarbons in real time, to obtain a holistic quantitative understanding of the dynamic evolution of full-spectrum MTO products, taking the selected MTO reaction as a prototypical case (see [Supporting Information](#) for details). As highlighted in [Fig. 2\(d\)](#), the expenditure of small percentage (e.g., ca. 6% in this work) of feedstock methanol carbon atoms per unit time to construct and maintain “coke” deposits in SAPO-34 confined cavities is imperative for sustaining a continuous high-efficient light olefins production, according to HCP mechanism [7] as well as the enhanced light olefins shape-selectivity by PAHs accumulation [52,53]. However, further extension and clustering of HCP species and the plethora of PAHs formation exacerbate MTO termination ([Fig. S10](#) and [Table S4](#)). This CAFD concept, encompassing and distinguishing between the main MTO reaction (targeted light olefins production catalyzed by HCP species) and coking process (evolution from HCP species to PAHs, [Fig. 2g](#)), quantitatively portrays the entire cradle-to-grave full-spectrum MTO products molecular evolutionary trajectory (fate, [Fig. 1](#)), and helps revisit and clarify the role of the requisite carbon footprints in each confined “coke” as reactive centers and/or local diffusion modifiers (especially of the long-stand yet less recognized end-product of carbon resources-cage-passing PAHs). More significantly, it emphasizes the necessity of resource utilization of PAHs, which is converted to CO₂ in conventional air combustion regeneration, to maximize the exploiting of carbon resources from, but not limited to C1 platform molecules.

Subsequently, double-bond equivalent (DBE) and C/H ratio were employed as descriptors to elucidate the molecular pathways of PAHs evolution ([Fig. 2h](#)). The relatively continuous carbon number (CN), DBE, and the rapidly elevated C/H ratio from Families A to D reveal that in-cage aromatic extension undergoes a complex reaction network, encompassing aromatic electrophilic substitution (alkylation), polyenyl side chain intramolecular cyclization, Diels-Alder reactions between aromatics and alkenes, intramolecular rearrangement, hydride transfers, among others, in line with a DBE step length (Δ DBE) of 3–4 ([Table S2](#)). These observations corroborated the gradual transform in the role of organic intermediates, from H-sufficient active HCP species as cocatalysts into H-deficient inactive coke precursors (PAH clusters) as deactivation initiator that can be accommodated in only one CHA cavity. For Families E to H, however, the carbon number and DBE distribution become discrete with a DBE step length leaping to 10–13, corresponding to phenanthrene (10) and pyrene (12), and the C/H ratio converges to 2, rather than a linear increase with DBE. These trends strongly suggest that the cage-passing PAHs speciation originates exclusively from direct coupling between soluble “cokes” that have been formed in adjacent cages; rather than from the cyclization of long side chain of one in-cage aromatics extending into another neighboring cavity, which often occurs when coking in the channel-structure zeolites, such as HZSM-5 [42,49], HBEA [43] and mordenite [54]. The complex evolution network of PAHs is, thus, more clearly interpreted at molecular level, that “coke” growth under the confinement of CHA architecture is initially inclined to ring extension until the size of in-cage aromatics evolves bulky enough (commonly pyrene, PAHs of the maximum size that can be accommodated in an individual *cha* cage [12]) to cater to the dimension and size of *cha* cavities, and then PAHs cage-passing clustering process would relay to dominate the “coke” family evolution, as depicted in the illustrative molecular routes outlined in [Fig. 2\(g\)](#). The unique PAHs self-coupling speciation under the special confinement of the connected cavity environments, and the quasi-quantized molecular evolution motif quantified with its inherent increasing iterative DBE step length, manifest the intriguing dynamic behavior of MTO and coking chemistry, and further immensely enriched the understanding of cavity-controlled molecular recognition concept and (product)

shape-selective principle in zeolite catalyzed hydrocarbons conversion.

2.2. Mechanistic pathways of cage-passing PAHs speciation

Having explicitly delineated the full-spectrum products molecular evolution trajectory and systematically quantifying the decisive roles of aromatic hydrocarbons, next we focus on the missing mechanistic interpretation of the cage-passing PAHs formation pathway. We anticipate that by using this knowledge, we would achieve a bottom-up approach to mitigating coking and catalyst deactivation.

In the magnified high-resolution MALDI FT-ICR mass spectrum of carbonaceous extracts obtained from the catalysts after MTO reaction for initial 24.5 min ([Fig. 3a](#)), apart from the mass signals that have been ascertained as coke Family E, namely 339, 353, 367, and 381 Da, an array of new signals with 2 Da heavier than the above main peaks were simultaneously captured. According to the isotopic shifts obtained from delicate isotope labeling experiments ([Fig. S11](#)), they were identified as naphthylpyrenylmethane (NPM, 342 Da) and its homologues. It should be noted that these weak signals rapidly decreased in intensity as reaction proceeded, and their ratio to the main peaks diminished to negligible extents at 46 min. Such transient feature, thus, permits us to infer the short-lived NPM species likely to be a potent intermediate in PAHs cage-passing clustering process.

Based on this experimental evidence, the following stepwise clustering mechanism is proposed, taking coke Family E as an illustrative example ([Scheme 1](#)). The reaction sequence starts with the methyl-naphthalene activation through hydride transfers, where some olefin products, such as propene or butene that are generated at high-efficient reaction stage and are occluded in the catalyst as the adsorbed MTO products at acid sites (isopropoxy or butoxy), act as the hydride acceptor. Alkoxy groups extract a hydride from the methyl group of methyl-naphthalene to form propane or butane and a positively charged MN carbonium ion or MN-alkoxide; while during the deactivation stage, methanol (methoxy) is potentially the main hydride acceptor, as evidenced by up to 60% of methane selectivity upon deactivation ([Fig. 2a](#)) and extremely high ¹³C incorporation for methane in transient ¹²C-/¹³C-methanol switch experiments ([Fig. 3b](#) and [Fig. S12](#)). These also provide possible origins of propane and butane at high-efficient stage and that of methane as the main product upon deactivation. Recent studies also showed that formaldehyde stemming from methanol hydrogen transfers or disproportionation accelerated coke formation [55–57]. In a side pathway, thus, MN-alkoxide can also be formed through the reaction of naphthalene and formaldehyde. This carbonium ion then adds to pyrene in the neighboring cage to form NPM (342 Da) with an extra proton at pyrene ring positions. Cross-link process (Step 1) is fulfilled with back-donation of proton to SAPO-34 framework. Thereafter, the formed NPM intermediate continues to undergo another consecutive series of hydride transfer, coupling and deprotonation reactions to complete 5-ring closure to form coke Family E (Step 2, clustering). Of note is that the mass difference, 2 Da between coke Family E and NPM, indicates that the PAHs precursor, NPM, goes through hydride transfers to realize inter-cage ring-closure in clustering process.

Then, the question arises as to how these highly condensed PAHs react. It is suggested that the excess chemical potential that could raise the energy level of the ground state of the adsorbed reactants and lessen free energy barrier is concentration-dependent when the sum of the charges of all products remains unvaried [58]. This allows us to surmise that the less mobility of the bulky aromatics under the confinement conferred by *cha* cavity reactors that induces the accumulation of retained bulky organics also leads to an enhanced excess chemical potential, which could

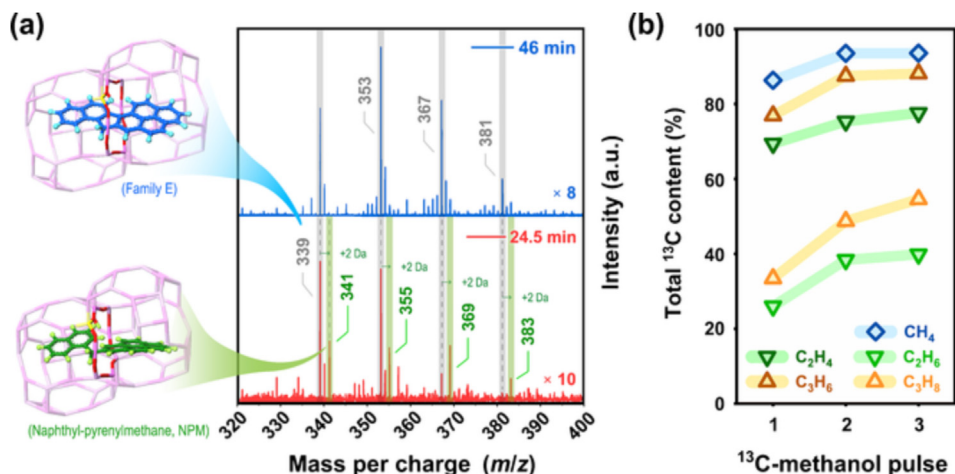
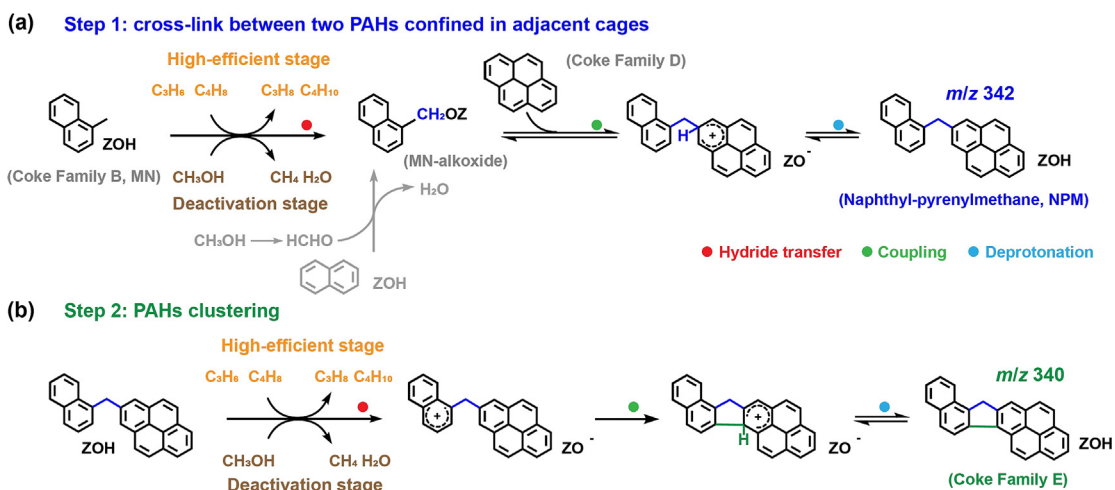


Fig. 3. Capture of plausible intermediates formed during cage-passing PAHs speciation. (a) Magnified MALDI FT-ICR mass spectra of extracts obtained from the catalysts after water cofeeding MTO reaction at 475 °C and WHSV of 1.5 h⁻¹ for 24.5 and 46 min, focusing on the 320–400 Da range, coupled with the illustrative molecular structures of cage-passing PAHs occupying two cages (Family E) and naphthyl-pyrenylmethane intermediates (NPM). Noteworthy, we stress that the illustrative molecular structures collected in this study are certainly not absolute, and they were meant to highlight the concept of cage-passing growth of PAHs, which also holds true when describing PAHs decomposition network (see below). (b) Total ¹³C content of effluent C₁–C₃ gas-phase products obtained by transient ¹²C-/¹³C-methanol switch experiments with ¹²C-methanol feeding for 196.5 min followed by 30 s, 90 s and 150 s of ¹³C-methanol feeding, respectively.



Scheme 1. Schematic illustration of the proposed stepwise PAHs cross-linked clustering pathways. Cage-passing PAHs speciation in HSAPO-34 undergoes first cross-link through methylene as molecular bridge between two aromatics inside adjacent cages (a) and sequentially PAHs clustering through 5-ring closure at inter-cage 8-ring apertures (b), taking coke Family E as an illustrative example.

further act as the driving force for the cage-passing PAHs formation via above steps. Concurrently, by using atom probe tomography (APT), the significant affinity between coke and Brønsted acid sites was directly identified at atomic level [59]. On the other hand, theoretical evidence suggested that the stabilizing π -H interactions can largely enhance aromatics occurrence probability at 8-rings [60]. Besides, π -interaction-induced spatial proximities between aromatics in the adjacent cages were also experimentally observed [61]. Thus, the long residence time of PAHs since being formed and confined in CHA cages may also augment the probability of this cross-linked clustering process. On the other hand, the stabilization of diaryl carbonium ions as well as their neutral counterparts could be attained not only by the use of larger cavities where spatial restrictions can be avoided, but specially by their fitting with the zeolite local environment whose limited voids could intensify host-guest interactions (mainly referring to dispersion and van der Waals interactions), rather than repulsion [62–67]. Thus, with the higher energy level of the ground state of confined PAH molecules, the relatively stabilized carbonium ion (MN-alkoxide) would

further reduce the activation energy of its own formation which might be the rate determining step in the overall cage-passing PAHs speciation scenarios. With all these cogent points in mind, we argue that the speciation of cage-passing PAHs in CHA materials with narrow pore opening through the stepwise hydride transfer involved process via bulky diaryl intermediates (such as NPM) is intuitively surprising but is plausible. In the confined environment, CHA zeolite surroundings guide cross-linking reactions of the aromatics generated and confined in each cavity, forming cage-passing PAHs traversing 8-ring apertures.

As shown in Fig. 2(c and e), the initial cage-passing PAHs content in methanol-water cofeeding reaction was much lower than that under pure methanol as feedstock [12], while the soluble “coke” signals were comparable, triggering us to speculate that this process for insoluble PAHs formation is more susceptible to water. To ensure these observations not derived from water dilution effect in methanol–water cofeeding reaction and to interrogate the effect of in situ produced water, we carefully designed the methanol–argon cofeeding experiments with consistent methanol

partial pressure and WHSV. In cofed water MTO reaction, 25% increase in coke content yet 40% increase in catalyst lifetime were observed (Fig. S13) cohered with the previous report [36], suggesting that certain amounts of water promote methanol conversion by inducing a more efficient use of the SAPO-34 crystal. Coincident with 12% and 40% increase in the formation rates of total coke and cage-passing PAHs respectively, 20% increase in initial insoluble coke proportion and a noticeable shift of dominating PAHs from coke Family F to heavier Family G were observed in argon cofeeding mode (Fig. S14). These results indicate that the entire domino cascade evolution network of confined hydrocarbons is conspicuously depressed by cofed water (Fig. 1). Besides, the remarkable disparities in cage-passing PAHs speciation reveal the more pronounced inhibition of PAHs cross-linked clustering by water than that of in-cage extension. Furthermore, in situ produced water proves not sufficient to compete to hinder cage-passing PAHs formation. In summary, these findings not only rule out the diluent effect of cofed water, but further yield new insights into why water cofeeding strategy is effective in prolonging catalyst lifetime. The prevailing water molecules that competitively occupy acid sites retard HCP species formation as well as subsequent in-cage extension and will more effectively suppress the spontaneous speciation of cage-passing PAH clusters by lessening the probability of inter-cage molecular bridge formation. In other words, water extends the working expectancy of active HCP species. To restrict and to enrich the confined hydrocarbons into HCP species range, according to our CAFD model (Fig. 2d), is beneficial for achieving a high-efficient autocatalytic methanol conversion. It should be noted in passing that the reduction in the size of cage-passing PAHs might also ameliorate local mass transfer blockage, which would further favor methanol diffusion at the single crystal scale.

2.3. Water-promoted PAHs decomposition mechanism in CHA materials and application in coked catalyst regeneration

As PAHs extension and clustering, as well as coking and catalyst deactivation (autocatalysis decaying) prove spontaneous and inevitable, decoding the molecular routes of the reverse process—PAHs decomposition and seeking for a more effective regeneration (autocatalysis recovering) strategy for coked catalysts are necessitated and highly demanded. This, according to the current carbon-neutral policy, is of even legal importance because coke is converted into large amounts of CO₂ in conventional air combustion regeneration (Fig. 1).

Another striking array of phenomena observed in water cofeeding MTO reaction suggested coke digestion under hydrothermal condition. For the deactivated catalyst after MTO reaction for 196.5 min (heavily-coked catalyst over which methanol conversion below 10%): (1) Continuous methanol–water cofeeding led to slight decrease of coke content while micropore volume concurrently was recovered (Fig. 2e and Fig. S4); (2) In parallel with the extinction of coke Families E to H, the two new groups of MS signals that germinated at 175 min dominated the insoluble coke range (Fig. 2c and Fig. S9), which were identified as lighter cage-passing PAHs analogues (occupying two and three cages, denoted as coke Families I and J respectively, Fig. S6); (3) The trends in the proportion of soluble and insoluble coke reversed (Fig. S10) and coke combustion temperature decreased (the maximum temperature of differential curves, $T_{G,max}$, that can reflect the nature of coke, i.e., the lower the $T_{G,max}$ the higher the H/C ratio of coke, Fig. S15); (4) An exceptionally high CO selectivity (>5%) was also detected (Fig. 2a) in water cofeeding reaction. With the knowledge obtained above that the extension and clustering of PAHs are inhibited by water, following this line of thought, we extrapolate that PAHs, especially the more water-vulnerable cage-passing coke

clusters, would become less stabilized under hydrothermal condition, and water-promoted low-temperature PAHs decomposition would occur in the same CHA constrained environment as their speciation.

To testify this hypothesis, we performed steam treatment-experiments by switching methanol feedstock to water at 196.5 min of MTO reaction with water feeding rate maintained consistent. As depicted in Figs. S16(d) and S17(d), a more pronounced shift in cage-passing PAHs speciation was captured within the initial 20 min of switching feedstock to water, accompanied with a slight increase in Families B and D in the soluble “coke” range. Synchronously, mass signals of hydroxyl-pyrene and its homologous that emerged in coked catalyst after 239.5 min of MTO reaction (Fig. S18) were intensified in the above steam treatment experiments. These results confirm that water tangibly participated in and accelerated the degrading of confined cage-passing PAHs and permit us to surmise that in-cage naphthyl- and pyrenyl-species as well as their oxygenated derivatives are the primary coke-degrading products. Note that all the preceding observations were not detected in methanol-argon cofeeding reactions (Fig. S13d) or when only feeding methanol [12], negating the ability of in situ produced water molecules to provoke PAHs cracking. In details, apart from the mass signals attributed to coke Family E (339, 353, 367 and 381 Da) and NPM species (341 and 355 Da), two new solitary signals at 326 and 328 Da emerged at 196.5 min in water cofeeding reaction and increased in intensity with steam treatment durations (Fig. 4a). Their molecular structures were tentatively identified as naphtho[1',2':3,4]cyclobuta[1,2-a]pyrene (NCP) and naphthyl-pyrene (NP). The occurrence of the latter as well as NPM signifies ring-opening processes of the 4-ring or 5-ring inter-cage local structures, while that of the former implies re-condensation. These intermediates are the potential precursors of naphthalene, pyrene and phenols. Additionally, a slight but monotonous increase in micropore volume was also observed with the decrease in coke content (Table S1), reaffirming the release of the blocked micropore voids by coke partial decoupling to allow for diffusion admittance.

After noticing coke partial degrading under atmospheric hydrothermal condition at 475 °C, we sought for more efficient hydrothermal conditions to reach water-promoted complete PAHs decomposition for catalyst regeneration. Further insights are acquired by inspecting the high-temperature and high-pressure profiles at 650 °C and water partial pressure of 2 MPa (Figs. S16a–c and S17a–c). After the identical shift in insoluble coke speciation and increase in naphthalene, signals of the dominating coke Families B, I and J continued to decrease in intensity and eventually vanished. These were well-supported by the significant reduction in coke content and synchronous substantial recovery in micropore volume (Fig. S19 and Table S5), as well as the continuous drop in coke air combustion temperature ($T_{G,max}$, Fig. S20). Released gas during complete PAHs decomposition were mainly composed of H₂, CO and CH₄, which can reach ca. 50, 40 and 7 vol%, respectively (Fig. S21 and Fig. 4e), signifying that coke scavenging occurred via a steam reforming-related mechanism. Notable is the absence of CO₂ in the effluents, which is of particular importance to the design of an ecofriendly future-generation catalyst regeneration strategy with zero CO₂ emissions in coke steam reforming, whereas coke air combustion into CO₂ is conventionally employed for industrial catalyst regeneration. The presence of a small fraction of exothermic methanation [68] (Fig. S22) might lower the onset temperature (475 °C) of PAHs degrading/decomposition in HSAPO-34 confined space.

Based on this experimental evidence, we sketched the following stepwise water-promoted PAHs decomposition mechanism. Under hydrothermal conditions, cage-passing multicore PAH clusters formed inside SAPO-34 confined space are more prone to, if not

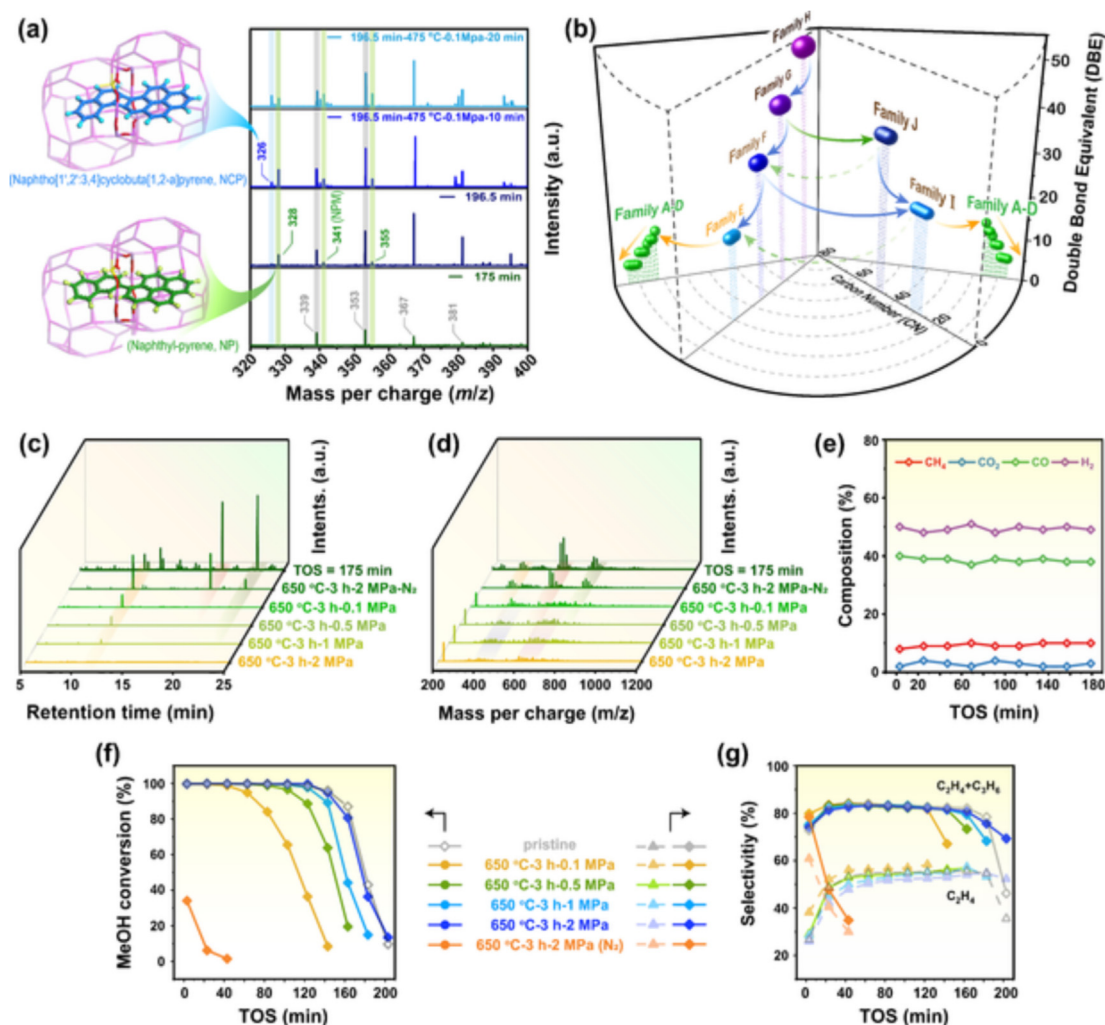
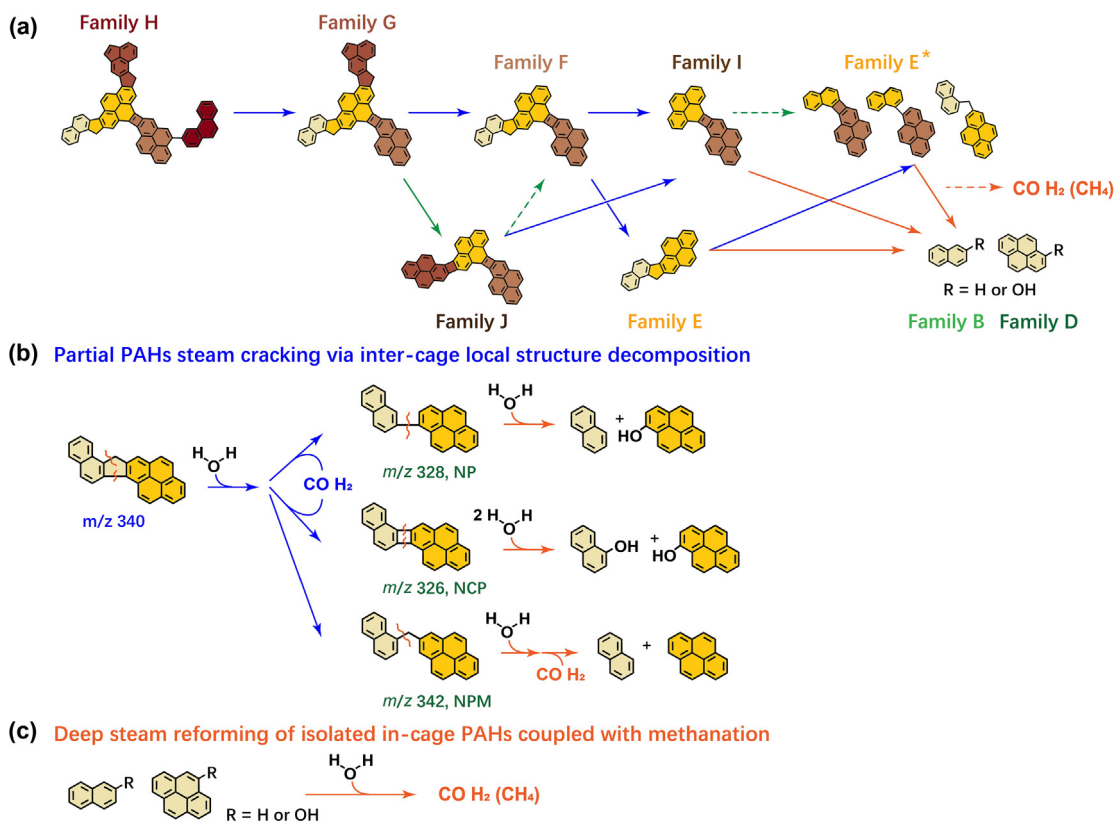


Fig. 4. Evolution of full-spectrum confined hydrocarbons during steam treatment and MTO performances over regenerated catalysts. (a) Magnified MALDI FT-ICR mass spectra of extracts obtained from the catalyst after 175 and 196.5 min of water cofeeding MTO reaction at 475 °C, and that after steam treatment for 10 and 20 min of the coked catalyst after water cofeeding MTO reaction for 196.5 min, coupled with the illustrative molecular structures of naphtho[1',2':3,4]cyclobuta[1,2-a]pyrene (NCP) and naphthyl-pyrene (NP). (b) 3D plot of molecular evolution route of full-spectrum PAHs decomposition with double bond equivalent and carbon number as descriptors. (c, d) Evolution of full-spectrum confined hydrocarbons in nitrogen and during steam treatment at 650 °C. (e) Gas composition during steam treatment at 650 °C under 2 MPa of the semi-deactivated MTO catalyst sample (after water cofeeding MTO reaction for 175 min, with methanol conversion at ca. 50%). The reactivity (f) and light olefins selectivity (g) of the fresh MTO catalyst and the semi-deactivated MTO catalyst after steam treatment at 650 °C for 3 h.

exclusively, being degraded into smaller sized analogues and in-cage structural units via local cracking of the inter-cage structures at 8-rings before deep steam reforming into H₂ and CO, as evidenced by the discrete DBE and CN in Fig. 4(b), rather than non-regioselective PAHs steam reforming, if so, the DBE and CN should appear continuous [37]. Taking Family E as an illustrative example, we elaborated the elementary routes (Scheme 2). Reaction sequence starts with water-induced selective C–C cleavage at inter-cage local structures for ring-opening to produce NCP and NP cracking intermediates, synchronously generating small fraction of H₂ and CO (Fig. 2a). In parallel, decomposition of these relatively labile antiaromatic local structures at 8-rings can also be provoked by in situ generated H₂ to produce NPM intermediate or to produce NP intermediate and CH₄. The hydrogenation ability of HSAPO-34 for PAHs has been demonstrated in the previous study [69]. Subsequently, the above three intermediates continue to undergo steam-degrading into in-cage aromatic structural units (mainly naphthalene and pyrene) and their oxygenated derivatives through further cleavage of C–C molecular bridge bond (Scheme 2b). These primary products are ultimately transformed in large quantities into H₂ and CO via deep steam reforming

(coupled with small fraction of methanation), which needs to be driven by higher temperatures and/or higher local steam pressure. Of note is that the re-condensations of in situ produced pyrene during high-temperature steam treatment would make the actual PAHs decomposition process in SAPO-34 a complex and cooperative cascade reaction network.

Thanks to the direct capture of the PAHs intermediates as well as the mapped comprehensive mechanistic network, we, in large part, achieved a full-spectrum molecular understanding of the PAHs decomposition in small-pore CHA materials, evolving from insoluble cross-linked cage-passing PAH clusters (Families E to J) to isolated cavity-confined soluble “coke” (mainly Families B and D), and eventually to H₂ and CO (feed for methanol synthesis) as illustrated in Fig. 1. This evolutionary trajectory *per se* provides an intuitive manifestation that coking and decoking evolution present opposite trajectories on specification in CHA confined space at the molecule level. Furthermore, the molecular structure of the aromatic intermediates and the molecular routes that are independent of the reaction condition indicate that the water-promoted PAHs decomposition is also cavity-controlled shape-selective process [12]. For MTO reaction, the chemical nature of coke structural



Scheme 2. Schematic illustration of the proposed water-promoted PAHs decomposition (PAHs steam cracking) mechanism. (a) Full molecular picture of the cascade cage-passing PAHs decomposition network in HSAPO-34 along the evolutionary trajectory. Blue arrows denote the local decomposition of inter-cage structures at 8-rings (cleavage of inter-cage molecular bridge). Green arrows denote the possible re-condensation events. Orange arrows denote the deep steam reforming (main reaction) and methanation of PAHs. The actual mechanistic details of the water-promoted coke decomposition network may be more complex than the catalytic portray illustrated here. (b, c) The proposed reaction sequence for stepwise water-promoted decomposition of cross-linked cage-passing PAHs, taking coke Family E as an illustrative example.

units is cavity-controlled; they spontaneously traverse the narrow 8-ring windows via the establishment of molecular bridges to realize cross-linked clustering. During steam cracking, the cleavage of the molecular bridge prevails. In virtue of the compelling self-coupling and decoupling behaviors of PAHs guest, we explicitly exemplify the shape-selectivity concept based on host–guest interactions in HSAPO-34-catalyzed methanol conversion reactions and deepen the molecular understanding of shape-selectivity catalysis from the view of coking and decoking. We posit that such a holistic elucidation of the important dynamic full-spectrum hydrocarbons from active to inactive and restoration of active centers at the molecule level would support and motivate the fascinating MTH chemistry.

Next, the catalytic performances of the regenerated catalysts after steaming were evaluated. As depicted in Fig. 4, MTO reactivity of the semi-deactivated catalyst prominently recovered after steam treatment at 650 °C and 2 MPa water partial pressure for 3 h, which rivaled that of the fresh catalyst. This is well-supported by the complete coke scavenging from the full-spectrum and the micropore volume being recovered to over 90% of that of the pristine catalyst (Fig. S19 and Table S5). MTO performances of the fully deactivated samples after steam treatment under varying conditions are supplemented in Figs. S23 and S24. For all deactivated samples, the MTO reactivity was recovered with increasing steam treatment temperatures, steaming time and steam partial pressures. During this procedure, ethene selectivity gradually decreased at the initial stage while propene selectivity increased, which strongly suggests that recovery of the diffusion admittance of reactants and products is realized by PAHs steam

cracking that occurs from the exterior to the interior of the catalyst particle. Also, by the results from comparative experiments under nitrogen (Fig. 4c and d), we ruled out the contribution of PAHs pyrolysis at high temperature.

By exploiting the mechanistic understanding of PAHs steam cracking, we finally arrived at a steam regeneration strategy for the important HSAPO-34 catalyzed MTO reaction, as illustrated in Fig. 1. A steam partial regeneration was recently reported by us [38]. The present work provides a molecular interpretation of the underlying mechanism. We discern the positive yet divergent roles of water: under MTO reaction conditions, water selectively quenches PAHs clustering against the formation of active HCP species, enhancing the catalyst lifetime; under regeneration conditions, water of a higher local concentration promotes the in situ decomposition of the formed PAHs in a stepwise manner, realizing a reversible evolution of the confined hydrocarbons as well as a concomitant recovery of catalyst reactivity. Notable is that all these trends present dynamic, conforming to the concept of autocatalysis in MTH chemistry, further enabling the in situ self-regulation of dynamic autocatalytic behavior as well as steam regeneration to be highly expected. Of more practical significance, in contrast to the carbon resources to count that have drained away in air combustion regenerations, H₂ and CO as the dominant products in this steam regeneration strategy further supplies the methanol synthesis industry [4], largely facilitating a circular carbon atom economy [70]. Of further note, CO₂ emission during coke (PAHs) scavenging is successfully avoided in this steam regeneration approach. This also provides a feasible and environment-benign strategy for the valorization and functionalization of coke that contains significant

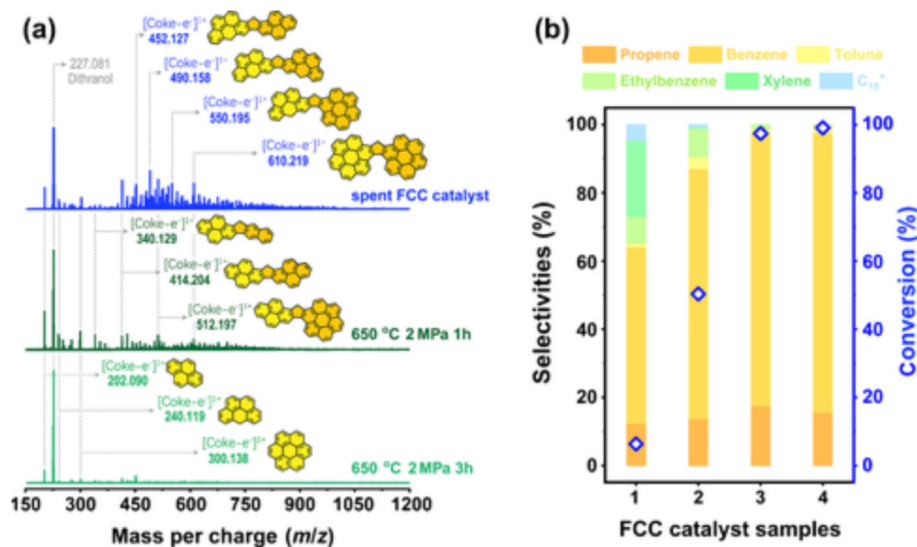


Fig. 5. PAHs steam cracking strategy implemented on the regeneration of the spent FCC catalyst. (a) MALDI FT-ICR mass spectra for extracted riganics obtained from the spent FCC catalysts and the samples after steam treatment at 650 °C under 2 MPa water partial pressure for 1 and 3 h as well as the deduced possible molecular structure of confined PAHs. The indicated molecular structures are representative examples of possible structures. (b) Isopropyl benzene (IPB) cracking performances at 300 °C and WHSV of 0.56 $\text{g}_{\text{IPB}}/\text{g}_{\text{cat}}\text{h}^{-1}$ over the spent FCC catalyst after calcined in air flow at 550 °C for 4 h (sample 4), the spent FCC catalysts after steam treatment at 650 °C and 2 MPa water partial pressure for 1 h (sample 2) and 3 h (sample 3) and the spent FCC catalyst (sample 1), respectively.

amounts of energy and carbon resource in the form of mixture of aromatics and PAHs, a form of carbon resource that is prevalent in all hydrocarbon conversions.

To investigate the generality of this strategy, we applied it to the regeneration of the spent fluid catalytic cracking (FCC) catalyst with coke content of 1.2 wt% (Fig. S26), which consists of the ultra-stable zeolite Y (FAU), a small proportion of zeolite ZSM-5, matrix and binder (see physicochemical properties in Fig. S25 and Table S6). The molecular evolution of the CCl_4 -extracted soluble coke during steam treatment were analyzed by GC-MS (Fig. S27), whereas the molecular structures of the insoluble coke with molar weight larger than 150 Da was determined based on the masses of the maximum peaks in MALDI FT-ICR mass spectra as well as the specific FAU topology ($11.2 \text{ \AA} \times 11.2 \text{ \AA} \times 11.2 \text{ \AA}$ supercages and $7.4 \text{ \AA} \times 7.4 \text{ \AA}$ pore apertures) and were shown in Fig. 5(a). For the spent FCC catalyst, the deduced coke molecules are found in complex structures with pyrene, 6H-benzo[cd]pyrene and coronene as coking units and 5-rings as molecular bridges, well-aligned with the more diffuse and crowded electron densities (high static disorder) mapped in the narrow space between adjoining supercages [71]. The predicted coking units are consistent with the GC-MS analysis of the extracts after dissolution-extraction experiments (Fig. S27). Other broad distributed MS signals are assigned to the coke formed in the mesopore voids of FCC catalyst particles. As steam treatment proceeded, the signals of the insoluble coke decreased in intensity and shifted towards smaller masses with structural units being dominated by pyrene. H_2 and CO as the main products were synchronously detected in the effluents (Fig. S28). Taking isopropyl benzene (IPB) cracking as a benchmark reaction, we found that the IPB conversion gradually recovered with the increase of steam treatment time, as shown in Fig. 5(b), and the catalytic performance of the regenerated sample after steam treatment at 2 MPa water partial pressure for 3 h drew level with that of the catalyst after air regeneration when coke species were completely scavenged. These results were well-supported by the substantially recovery in both micropore and mesopore volume (Table S6). It should be noted in passing that ^{27}Al MAS NMR spectra of the spent FCC catalysts before and after steam regenerations remained almost identical, as shown in Fig. S29, indicative of no noticeable occurrence of zeolite dealumination during steam treat-

ment (an irreversible loss of acidic sites would occur otherwise [72]). As noted, the marked applicability of the steam regeneration strategy in both FCC and MTO processes, the former of which is the main chemical process in oil refining for production of gasoline and propylene [72], would tangibly curb carbon emissions per unit of output in the hard-to-abate chemical industrial sectors. Further, the produced H_2 by coke valorization would supply the burgeoning CO_2 hydrogenation process [73–77].

3. Conclusions

By exploiting the state-of-the-art MALDI FT-ICR MS, this work unambiguously unveils the long-pursued missing fingerprints on the mechanistic pathways for the formation and water-promoted decomposition of the cross-linked cage-passing PAHs in the industrially important HSAPO-34 catalyzed methanol conversion reaction, whereby the molecule-level deciphering of the symmetrical and reversible evolution trajectory of full-spectrum hydrocarbons is fulfilled, and the real-time carbon resource footprints distribution for all the MTO products including PAH family is quantitatively tracked. Cage-passing PAHs speciation originates exclusively from the direct coupling of soluble “coke” formed and confined in adjacent cages, while its decomposition into in-cage HCP species initiates with the selective cracking of inter-cage local structures. Based on the molecule-resolved mechanistic understanding of coking and decoking chemistry in zeolite catalysis obtained in this work, we advance the classic deactivation mechanism by proposing that deactivation of CHA materials occurs through local cage blocking, triggered by long-chain polyene and in-cage aromatic units, and with their spontaneous cross-linked coupling, accelerated by the cage-passing PAH clusters. The dynamic deactivation motif is the macroscopical manifestation of the molecular evolution of full-spectrum hydrocarbons (PAHs) in a dynamic and autocatalytic manner in the confined space, which embodies the fascinating shape-selectivity catalysis concept based on host-guest interactions in MTH chemistry. By elucidating and leveraging the positive yet divergent outcomes of water that cofed water selectively quenches PAHs clustering against the formation of active HCP species under reaction conditions, while water of a

higher local concentration facilitates the catalyst regeneration by in situ decomposition of the formed PAHs, the rapid CHA catalyst deactivation is retarded and MTO reactivity is restored. We, finally, arrive at a steam regeneration strategy with valuable H₂ and CO as dominant products, mingling resource utilization of PAHs and avoiding CO₂ emission from combustion. The generality validated in other important hydrocarbon conversions, such as FCC process, promises it a potent and sustainable regeneration approach that will potentially contribute to carbon neutrality in the chemical sector.

This work, as a paradigm, is dedicated to feeding back and contributing to the development of important chemical processes involving coking deactivation and regeneration from the bottom up by our fundamental understanding of coking and decoking chemistry to achieve new technological developments and breakthroughs in low-carbon catalytic processes.

Experimental section

Experimental details can be found in the [Supporting Information](#).

Declaration of competing interest

The authors declare that they have no known competing financial interests or personal relationships that could have appeared to influence the work reported in this paper.

Acknowledgments

The authors thank the financial support from the National Natural Science Foundation of China (21991092, 21991090, 22022202, 21972142, 21902153, 21974138), the Chinese Academy of Sciences (QYZDY-SSW-SC024) and the Dalian Institute of Chemical Physics (DICP I201926, DICP I201947). We wish to acknowledge Dr. Lihong Wan for the support in MALDI FT-ICR mass spectra analysis. We acknowledge Dr. Wenna Zhang in Dalian Institute of Chemical Physics, Chinese Academy of Sciences, and Dr. Zhiqiang Liu and Dr. Wei Chen in Wuhan Institute of Physics and Mathematics, Chinese Academy of Sciences for the fruitful discussions in reaction mechanisms. We thank Dr. Yanli He in Dalian Institute of Chemical Physics, Chinese Academy of Sciences for the support in general characterization of spent catalysts. We also thank Dr. Xin Su in Dalian Institute of Chemical Physics, Chinese Academy of Sciences for providing the FCC catalyst samples.

Appendix A. Supplementary data

Supplementary data to this article can be found online at <https://doi.org/10.1016/j.jechem.2022.09.014>.

References

- [1] C.H. Bartholomew, M.D. Argyle, *Catalysts* 5 (2015) 949–954.
- [2] M. Guisnet, Deactivation and Regeneration of Zeolite Catalysts (2011) 217–231.
- [3] U. Olsbye, S. Svelle, M. Børjgen, P. Beato, T.V.W. Janssens, F. Joensen, S. Bordiga, K.P. Lillerud, *Angew. Chem. Int. Ed.* 51 (2012) 5810–5831.
- [4] P. Tian, Y. Wei, M. Ye, Z. Liu, *ACS Catal.* 5 (2015) 1922–1938.
- [5] M. Yang, D. Fan, Y. Wei, P. Tian, Z. Liu, *Adv. Mater.* 31 (2019) 1902181.
- [6] U. Olsbye, S. Svelle, K.P. Lillerud, Z.H. Wei, Y.Y. Chen, J.F. Li, J.G. Wang, W.B. Fan, *Chem. Soc. Rev.* 44 (2015) 7155–7176.
- [7] I. Yarulina, A.D. Chowdhury, F. Meirer, B.M. Weckhuysen, J. Gascon, *Nat. Catal.* 1 (2018) 398–411.
- [8] J. Zhong, J. Han, Y. Wei, Z. Liu, *J. Catal.* 396 (2021) 23–31.
- [9] J.F. Haw, W. Song, D.M. Marcus, J.B. Nicholas, *Accounts Chem. Res.* 36 (2003) 317–326.
- [10] S. Xu, Z. Zhi, J. Han, W. Zhang, X. Wu, T. Sun, Y. Wei, Z. Liu, in: C. Song (Ed.), *Advances in Catalysis*, Academic Press, New York, 2017, pp. 37–122.
- [11] D. Mores, E. Stavitski, M.H.F. Kox, J. Kornatowski, U. Olsbye, B.M. Weckhuysen, *Chem.-Eur. J.* 14 (2008) 11320–11327.
- [12] N. Wang, Y. Zhi, Y. Wei, W. Zhang, Z. Liu, J. Huang, T. Sun, S. Xu, S. Lin, Y. He, A. Zheng, Z. Liu, *Nat. Commun.* 11 (2020) 1079.
- [13] S. Gao, S. Xu, Y. Wei, Q. Qiao, Z. Xu, X. Wu, M. Zhang, Y. He, S. Xu, Z. Liu, *J. Catal.* 367 (2018) 306–314.
- [14] P. Magnoux, P. Roger, C. Canaff, V. Fouche, N.S. Gnepe, M. Guisnet, in: *Studies in Surface Science and Catalysis*, Elsevier, Amsterdam, 1987, pp. 317–330.
- [15] M. Børjgen, F. Bonino, S. Kolboe, K.-P. Lillerud, A. Zecchina, S. Bordiga, *J. Am. Chem. Soc.* 125 (2003) 15863–15868.
- [16] W. Dai, G. Wu, L. Li, N. Guan, M. Hunger, *ACS Catal.* 3 (2013) 588–596.
- [17] Y.T. Chua, P.C. Stair, *J. Catal.* 213 (2003) 39–46.
- [18] P.M. Allotta, P.C. Stair, *ACS Catal.* 2 (2012) 2424–2432.
- [19] M. Signorile, D. Rojo-Gama, F. Bonino, P. Beato, S. Svelle, S. Bordiga, *Phys. Chem. Chem. Phys.* 20 (2018) 26580–26590.
- [20] H. An, F. Zhang, Z. Guan, X. Liu, F. Fan, C. Li, *ACS Catal.* 8 (2018) 9207–9215.
- [21] W. Wang, A. Buchholz, M. Seiler, M. Hunger, *J. Am. Chem. Soc.* 125 (2003) 15260–15267.
- [22] D. Xiao, S. Xu, N.J. Brownbill, S. Paul, L.-H. Chen, S. Pawsey, F. Aussenac, B.-L. Su, X. Han, X. Bao, Z. Liu, F. Blanc, *Chem. Sci.* 9 (2018) 8184–8193.
- [23] D.M. McCann, D. Lesthaeghe, P.W. Kletniaks, D.R. Guenther, M.J. Hayman, V. Van Speybroeck, M. Waroquier, J.F. Haw, *Angew. Chem. Int. Ed.* 47 (2008) 5179–5182.
- [24] W. Zhang, Y. Zhi, J. Huang, X. Wu, S. Zeng, S. Xu, A. Zheng, Y. Wei, Z. Liu, *ACS Catal.* 9 (2019) 7373–7379.
- [25] J. Li, Z. Wei, Y. Chen, B. Jing, Y. He, M. Dong, H. Jiao, X. Li, Z. Qin, J. Wang, W. Fan, *J. Catal.* 317 (2014) 277–283.
- [26] A. Comas-Vives, M. Valla, C. Copéret, P. Sautet, *ACS Central Sci.* 1 (2015) 313–319.
- [27] A.D. Chowdhury, K. Houben, G.T. Whiting, M. Mokhtar, A.M. Asiri, S.A. Al-Thabaiti, S.N. Basahel, M. Baldus, B.M. Weckhuysen, *Angew. Chem. Int. Ed.* 55 (2016) 15840–15845.
- [28] Y. Liu, S. Müller, D. Berger, J. Jelic, K. Reuter, M. Tonigold, M. Sanchez-Sanchez, J.A. Lercher, *Angew. Chem. Int. Ed.* 55 (2016) 5723–5726.
- [29] X. Wu, S. Xu, W. Zhang, J. Huang, J. Li, B. Yu, Y. Wei, Z. Liu, *Angew. Chem. Int. Ed.* 56 (2017) 9039–9043.
- [30] Y. Chu, X. Yi, C. Li, X. Sun, A. Zheng, *Chem. Sci.* 9 (2018) 6470–6479.
- [31] C. Wang, Y. Chu, J. Xu, Q. Wang, G. Qi, P. Gao, X. Zhou, F. Deng, *Angew. Chem. Int. Ed.* 57 (2018) 10197–10201.
- [32] L. Yang, T. Yan, C. Wang, W. Dai, G. Wu, M. Hunger, W. Fan, Z. Xie, N. Guan, L. Li, *ACS Catal.* 9 (2019) 6491–6501.
- [33] Q. Qian, C. Vogt, M. Mokhtar, A.M. Asiri, S.A. Al-Thabaiti, S.N. Basahel, J. Ruiz-Martínez, B.M. Weckhuysen, *ChemCatChem* 6 (2014) 3396–3408.
- [34] E. Borodina, H.S.H. Kamaluddin, F. Meirer, M. Mokhtar, A.M. Asiri, S.A. Al-Thabaiti, S.N. Basahel, J. Ruiz-Martínez, B.M. Weckhuysen, *ACS Catal.* 7 (2017) 5268–5281.
- [35] J. Goetze, F. Meirer, I. Yarulina, J. Gascon, F. Kapteijn, J. Ruiz-Martínez, B.M. Weckhuysen, *ACS Catal.* 7 (2017) 4033–4046.
- [36] K. De Wispelaere, C.S. Wondergem, B. Ensing, K. Hemelsoet, E.J. Meijer, B.M. Weckhuysen, V. Van, Speybroeck, J., Ruiz-Martínez, *ACS Catal.* 6 (2016) 1991–2002.
- [37] J. Ashok, N. Dewangan, S. Das, P. Hongmanorom, M.H. Wai, K. Tomishige, S. Kawi, *Fuel Process. Technol.* 199 (2020) 106252.
- [38] J. Zhou, M. Gao, J. Zhang, W. Liu, T. Zhang, H. Li, Z. Xu, M. Ye, Z. Liu, *Nat. Commun.* 12 (2021) 17.
- [39] D. Rojo-Gama, S. Etemadi, E. Kirby, K.P. Lillerud, P. Beato, S. Svelle, U. Olsbye, *Faraday Discuss.* 197 (2017) 421–446.
- [40] C. Wang, X. Sun, J. Xu, G. Qi, W. Wang, X. Zhao, W. Li, Q. Wang, F. Deng, *J. Catal.* 354 (2017) 138–151.
- [41] G. Ye, H. Wang, X. Duan, Z. Sui, X. Zhou, M.-O. Coppens, W. Yuan, *AlChE J.* 65 (2019) 140–150.
- [42] S. Müller, Y. Liu, M. Vishnuvarthan, X. Sun, A.C. van Veen, G.L. Haller, M. Sanchez-Sanchez, J.A. Lercher, *J. Catal.* 325 (2015) 48–59.
- [43] L. Pinard, S. Hamieh, C. Canaff, F. Ferreira Madeira, I. Batonneau-Gener, S. Maury, O. Delpoux, K. Ben Tayeb, Y. Pouilloux, H. Vezin, *J. Catal.* 299 (2013) 284–297.
- [44] B. Arstad, A. Lind, J.H. Cavka, K. Thorshaug, D. Akporiaye, D. Wragg, H. Fjellvåg, A. Grønvdal, T. Fuglerud, *Microporous Mesoporous Mat.* 225 (2016) 421–431.
- [45] I. Lezcano-Gonzalez, E. Campbell, A.E.J. Hoffman, M. Bocus, I.V. Sazanovich, M. Towrie, M. Agote-Aran, E.K. Gibson, A. Greenaway, K. De Wispelaere, V. Van Speybroeck, A.M. Beale, *Nat. Mater.* 19 (2020) 1081–1087.
- [46] Y. Wei, J. Li, C. Yuan, S. Xu, Y. Zhou, J. Chen, Q. Wang, Q. Zhang, Z. Liu, *Chem. Commun.* 48 (2012) 3082–3084.
- [47] L. Qi, J. Li, L. Wang, C. Wang, L. Xu, Z. Liu, *Catal. Sci. Technol.* 7 (2017) 2022–2031.
- [48] J.R. Anderson, Q.N. Dong, Y.F. Chang, R.J. Western, *J. Catal.* 127 (1991) 113–127.
- [49] S. Lee, M. Choi, *J. Catal.* 375 (2019) 183–192.
- [50] J.T.C. Wennmacher, S. Mahmoudi, P. Rzepka, S.S. Lee, T. Gruene, V. Paunovic, J. A. van Bokhoven, *Angew. Chem. Int. Ed.* (2022) e202205413.
- [51] S. Ilias, A. Bhan, *ACS Catal.* 3 (2013) 18–31.
- [52] P. Bollini, A. Bhan, *ChemPhysChem* 19 (2018) 479–483.
- [53] J. Zhou, Y. Zhi, J. Zhang, Z. Liu, T. Zhang, Y. He, A. Zheng, M. Ye, Y. Wei, Z. Liu, *J. Catal.* 377 (2019) 153–162.
- [54] N. Chaouati, A. Soualah, M. Chater, M. Tarighi, L. Pinard, *J. Catal.* 344 (2016) 354–364.

- [55] Y. Liu, F.M. Kirchberger, S. Müller, M. Eder, M. Tonigold, M. Sanchez-Sanchez, J. A. Lercher, *Nat. Commun.* 10 (2019) 1462.
- [56] W. Wen, S. Yu, C. Zhou, H. Ma, Z. Zhou, C. Cao, J. Yang, M. Xu, F. Qi, G. Zhang, Y. Pan, *Angew. Chem. Int. Ed.* 59 (2020) 4873–4878.
- [57] B.L. Foley, B.A. Johnson, A. Bhan, *ACS Catal.* 11 (2021) 3628–3637.
- [58] N. Pfriem, P.H. Hintermeier, S. Eckstein, S. Kim, Q. Liu, H. Shi, L. Milakovic, Y. Liu, G.L. Haller, E. Baráth, Y. Liu, J.A. Lercher, *Science* 372 (2021) 952–957.
- [59] J.E. Schmidt, L. Peng, A.L. Paioni, H.L. Ehren, W. Guo, B. Mazumder, D.A. Matthijs de Winter, Ö. Attila, D. Fu, A.D. Chowdhury, K. Houben, M. Baldus, J.D. Poplawsky, B.M. Weckhuysen, *J. Am. Chem. Soc.* 140 (2018) 9154–9158.
- [60] P. Cnudde, E.A. Redekop, W. Dai, N.G. Porcaro, M. Waroquier, S. Bordiga, M. Hunger, L. Li, U. Olsbye, V. Van Speybroeck, *Angew. Chem. Int. Ed.* 60 (2021) 10016–10022.
- [61] C. Wang, M. Hu, Y. Chu, X. Zhou, Q. Wang, G. Qi, S. Li, J. Xu, F. Deng, *Angew. Chem. Int. Ed.* 59 (2020) 7198–7202.
- [62] L.A. Clark, M. Sierka, J. Sauer, *J. Am. Chem. Soc.* 125 (2003) 2136–2141.
- [63] L.A. Clark, M. Sierka, J. Sauer, *J. Am. Chem. Soc.* 126 (2004) 936–947.
- [64] J. Huang, Y. Jiang, V.R.R. Marthala, M. Hunger, *J. Am. Chem. Soc.* 130 (2008) 12642–12644.
- [65] E.M. Gallego, M.T. Portilla, C. Paris, A. León-Escamilla, M. Boronat, M. Moliner, A. Corma, *Science* 355 (2017) 1051–1054.
- [66] C. Li, C. Paris, J. Martínez-Triguero, M. Boronat, M. Moliner, A. Corma, *Nat. Catal.* 1 (2018) 547–554.
- [67] V.J. Margarit, M. Osman, S. Al-Khattaf, C. Martínez, M. Boronat, A. Corma, *ACS Catal.* 9 (2019) 5935–5946.
- [68] C. Vogt, M. Monai, G.J. Kramer, B.M. Weckhuysen, *Nat. Catal.* 2 (2019) 188–197.
- [69] X. Zhao, J. Li, P. Tian, L. Wang, X. Li, S. Lin, X. Guo, Z. Liu, *ACS Catal.* 9 (2019) 3017–3025.
- [70] G.A. Olah, *Beyond Oil and Gas: The Methanol Economy* *Angew. Chem. Int. Ed.* 44 (18) (2005) 2636–2639.
- [71] K. Kim, T. Lee, Y. Kwon, Y. Seo, J. Song, J.K. Park, H. Lee, J.Y. Park, H. Ihee, S.J. Cho, R. Ryoo, *Nature* 535 (2016) 131–135.
- [72] E.T.C. Vogt, B.M. Weckhuysen, *Chem. Soc. Rev.* 44 (2015) 7342–7370.
- [73] M. Aresta, A. Dibenedetto, A. Angelini, *Chem. Rev.* 114 (2014) 1709–1742.
- [74] B.M. Tackett, E. Gomez, J.G. Chen, *Nat. Catal.* 2 (2019) 381–386.
- [75] X. Jiang, X. Nie, X. Guo, C. Song, J.G. Chen, *Chem. Rev.* 120 (2020) 7984–8034.
- [76] D. Wang, Z. Xie, M.D. Porosoff, J.G. Chen, *Chem* 7 (2021) 2277–2311.
- [77] W. Wang, S. Wang, X. Ma, J. Gong, *Chem. Soc. Rev.* 40 (2011) 3703–3727.